

# A cyclic model for pressure insensitive soil

M.R. Hossain<sup>1</sup>, M.S.A. Siddiquee<sup>1\*</sup>, F. Tatsuoka<sup>2</sup>

<sup>1</sup>*Department of Civil Engineering  
Bangladesh University of Engineering and Technology, Dhaka 1000, Bangladesh*  
<sup>2</sup>*Tokyo University of Science, Noda shi, Chiba, Japan*

---

## Abstract

Geotechnical structures usually undergo cyclic loading during its lifetime of service. Bridge piers, abutments are very susceptible to cyclic loading. It has been a long standing problem to solve the cyclic loading phenomena by a reasonably accurate cyclic model. In this paper, a novel cyclic model is developed by extending the one-dimensional Masing's rule to general stress-space (3D). The cyclic behavior is simulated by introducing a new framework in which the origin of the stress-strain space is shifted to the instantaneous stress point while the direction of the loading is reversed. A hyperbolic growth function for isotropic strain hardening is used and Rowe's stress-dilatancy is implemented for the material with slight modification for cyclic loading. No new concept for hardening is introduced here, but the old isotropic hardening rule is applied in an efficient manner to simulate the behavior of material under cyclic loading.

**Keywords:** cyclic loading, elastoplastic model, Masing's rule.

---

## 1. Introduction

Soils are often subjected to transient and cyclic loading such as that induced by road traffic or by wind and wave action on bridges. Earthquakes provide additional examples of transient loading. To understand more deeply the response of soil to such loading it is necessary to account for its changing properties in the course of cyclic deformation and its inelastic behavior resulting in progressive dilation and associated pore pressure change.

Starting from pioneering work by Druker and Prager (1952), various improvements, extensions and alternative soil plasticity theories have been proposed. In this process the second author has proposed a novel model for the monotonic loading of geomaterial and implemented the model for multi-element FE code (Siddiquee 1994). The cyclic evaluation of the material is modeled through kinematic hardening, isotropic hardening

---

\* Email: sid@ce.buet.ac.bd

or a combination of both. The cyclic evaluation of extended Masing behavior is very difficult to model through the kinematic hardening (Hossain 2005, Montáns 2000). Masing's rule states that the unloading curve keeps a homological ratio of two to monotonic one. It has been experimentally observed that this rule holds closely in most materials. The extension of this rule, also observed in most materials, is that the modeling process takes place through the initial monotonic curve or through previous reloading ones when they are intersected. The numerical simulation of this rule from isotropic and kinematic hardening requires difficult-to-obtain variable combinations of both hardening types.

The objective of the present study is therefore to develop a method to simulate the cyclic stress-strain relation of sand subjected to irregular cyclic loading history. The proposed model has the advantage that it has a direct relevance to Masing's rule. The cycle will close and the monotonic curve will be recovered after the previous threshold has been surpassed. The computational cost will be substantially smaller than that of traditional multi-surface models and the accuracy will usually be better.

## 2. Formulation of the constitutive relation

An isotropic strain hardening single surface model is formulated within a new framework to simulate the cyclic behavior of geo-material. Hardening part of the model is achieved through a hyperbolic equation, which can model the non-linear stress-strain relationship. The cyclic behavior is simulated by introducing a new framework in which the origin of the stress-strain space is shifted to the instantaneous stress point while the direction of the loading is reversed. Then the yield surface again grows isotropically from the new origin.

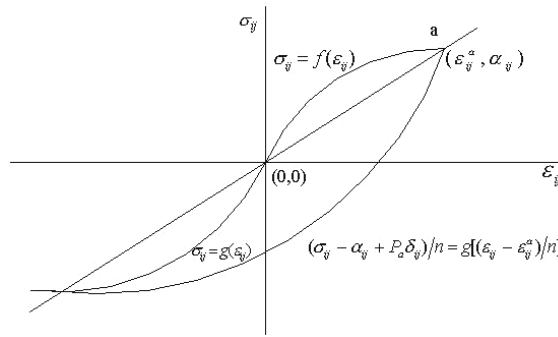


Fig. 1. Framework for cyclic loading

Here during loading the stress state moves from the origin to the point 'a' where  $\sigma_{ij} = \alpha_{ij}$  for a corresponding strain  $\epsilon_{ij}^a$  following a loading curve  $\sigma_{ij} = f(\epsilon_{ij})$ . Now when the unloading starts the origin is shifted to  $\alpha_{ij}$  and the direction of the stress tensor  $\sigma_{ij}$  and strain tensor  $\epsilon_{ij}$  is reversed. Now all the calculation is made from the new origin and yield surface grows isotropically from it. And the unloading curve follows the equation  $(\sigma_{ij} - \alpha_{ij} + P_a \delta_{ij}) / n = g[(\epsilon_{ij} - \epsilon_{ij}^a) / n]$  where  $n$  is ratio between unloading curve to the unloading skeleton curve. It is obtained by using a proportionality rule where a straight line is drawn from the point of stress reversal passing the origin O to intersect the

unloading skeleton curve and thus finds the value of  $n$ . If the loading and unloading skeleton curves are similar in shape,  $n$  is equal to two, which is stated by Masing's rule. If the confining pressure at O is  $P_0$  and at Point a it is  $P_0 + \Delta P$ , then set  $P_a$  as  $P_0 - \Delta P$ . This confining pressure ensures a smooth connection between the unloading curve and the unloading skeleton curve.

When the unloading curve intersects the unloading skeleton curve, origin is restored to the original position and the stress-strain relationship is found by the hyperbolic relationship of  $\sigma_{ij} = g(\varepsilon_{ij})$ . Thus a close hysteretic stress-strain relation is found giving the most accurate material response. Now by employing the drag rule we can simulate the increase in stress amplitude for same strain value during cyclic loading.

### 3. Yield function and plastic potential

Any strain-hardening model needs the description of a set of continuous yield and plastic potential surface (in case of non associative flow rule). As in this study mostly granular material will be dealt with, so the yield function will follow the material suitability. All point differentiable smooth Drucker-Prager failure criteria for yield function is chosen. The yield function ( $f$ ) and plastic potential function ( $\phi$ ) are given by,

$$f = \eta I_1 + \sqrt{J_{2D}} \quad (1)$$

$$\phi = \xi I_1 + \sqrt{J_{2D}} \quad (2)$$

where,

$$\eta = \frac{2 \sin \varphi_{mob}}{\sqrt{3}(3 - \sin \varphi_{mob})} \quad (3)$$

$$\xi = \frac{2 \sin \psi}{\sqrt{3}(3 - \sin \psi)} \quad (4)$$

$\varphi_{mob}$  = Mobilized angle of friction,  $\psi$  = Angle of dilatancy

### 4. The growth function

The growth function (Tanaka) expressed as follows was used,

$$\eta = \left[ \frac{2\sqrt{\kappa\kappa_f}}{\kappa + \kappa_f} \right]^m \eta_p \quad (\kappa \leq \kappa_f) \quad (5)$$

where  $m$  and  $\kappa$  are material constants and  $\eta_p$  is the value of  $\eta$  at the peak state.

### 5. Modification of the original Masing's rule

Here  $\tau = f(\gamma)$  represents the primary loading and unloading curves that are symmetric about the origin i.e.,  $f(-\gamma) = -f(\gamma)$ . When the loading direction is reversed at point 'a' ( $\tau_a, \gamma_a$ ), the unloading curve is given as:  $(\tau - \tau_a)/n = f[(\gamma - \gamma_a)/n]$

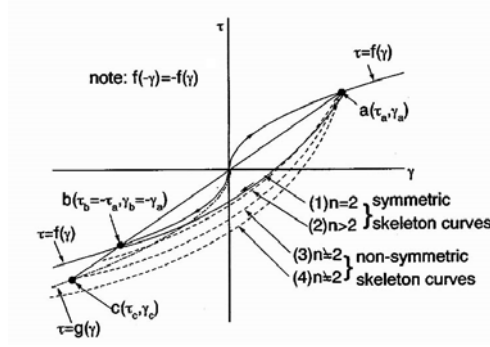


Fig. 2. Schematic diagram explaining proportional rule (Tatsuaka et al., 1999)

where  $n=2$ . In this case, the unloading curve joins the unloading skeleton curve at the symmetric point 'b' ( $\tau_b, \gamma_b$ ) with  $\tau_b = -\tau_a$  and  $\gamma_b = -\gamma_a$ . On the other hand, many experimental results show that the unloading curve from point 'a' does not join the skeleton curve at point 'b'. In addition, the primary loading and unloading curves could be largely non-symmetric. In this case, two different functions  $\tau = f(\gamma)$  and  $\tau = g(\gamma)$  should be assigned for loading and unloading curves. It could be assumed that the unloading curve from point 'a' in this case is given as,

$$(\tau - \tau_a)/n = g[(\gamma - \gamma_a)/n]$$

where point 'c' ( $\tau_c, \gamma_c$ ) = intersection of straight line passing the reversing Point a and the origin and the unloading primary curve  $\tau = g(\gamma)$ . For unloading curve to join the primary unloading curve at point 'c', the power  $n$  should be equal to  $-(\tau - \tau_c)/\tau_c (\geq 0)$ , which is usually different from two and may not be constant during cyclic loading. The value of  $n$  is determiner by proportional rule (Tatsuaka et al. 1999, 2003).

For the current model the relationship between  $\eta$  and the plastic hardening parameter  $\mathcal{K}$  is used because the  $\eta$ - $\mathcal{K}$  relations are much more symmetric and simpler to model with. Now, by moving the origin to the point of reversal for the unloading curve we get,

$$\eta = n \left[ \frac{2\sqrt{\mathcal{K}\mathcal{K}_f}}{n} \right]^m \eta_p \quad (6)$$

where  $\mathcal{K}$  is calculated from the new origin.

## 6. Modeling hysteretic stress-strain relationship (proportional rule)

The proportional rule consists of external and internal rules. Upon the reversal of loading direction, either external or internal rule is chosen for a given loading history based on the largeness of the current value of  $\mathcal{K}$  relative to instantaneous maximum and minimum value of  $\mathcal{K}$  as  $\mathcal{K}_{\max}$  and  $\mathcal{K}_{\min}$ . To keep continuity between external rule and internal rule, it is assumed that a pair of points having coordinates  $\mathcal{K}_{\max}$  and  $\mathcal{K}_{\min}$  is always

located on opposite side of the origin O on a straight line passing the origin. The meaning of  $\kappa_{\min}$  and  $\kappa_{\max}$  is explained below:

1. Suppose that loading starts from the origin and continue until Point A. At Point A,  $\kappa_{\max}$  = the maximum value of  $\kappa$  ever achieved by loading =  $\kappa_A$ . Accordingly,  $\kappa_{\max}$  at Point B (located along the first unloading curve from Point A) =  $\kappa_A$ . When the current  $\kappa$  value becomes larger than the previous value of  $\kappa_{\max}$  (i.e., when  $\kappa > \kappa_{\max} = \kappa_A$ ), the previous value of  $\kappa_{\max}$  is replaced by the instantaneous  $\kappa$  value.
2. The  $\kappa_{\min}$  value is defined as the smaller value of (a) the smallest value of  $\kappa$  ever attained during unloading and (b) the  $\kappa$  value at the intersection of the straight line starting from the point of  $\kappa_{\max}$  and passing the origin O with the unloading skeleton curve  $\eta = g(\kappa)$ . The  $\kappa_{\min}$  value of Point B =  $\kappa_C$  ( $\kappa$  at Point C), corresponding to Point A.
3. The  $\kappa_{\max}$  value is defined as larger value of (a) the largest value of  $\kappa$  ever attained by loading and (b) the value of  $\kappa$  at the intersection of the straight line starting from the point of  $\kappa_{\min}$  and passing the origin O with the loading skeleton curve  $\eta = f(\kappa)$ .

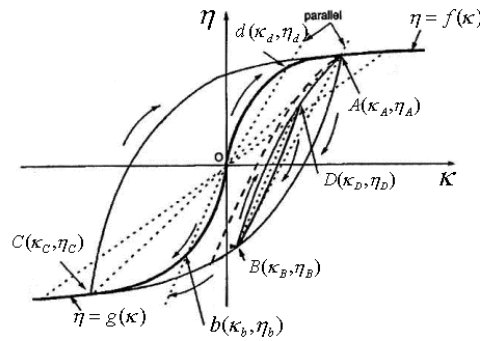


Fig. 3. Details of proportional rule

The rules to obtain the hysteretic stress-strain relationship for cyclic loading are described below, referring to Figs. 3 and 4:

1. Stress-strain curves for reloading and so on are obtained as follows:
  - When unloading is reversed to reloading while renewing the  $\kappa_{\min}$  value to the instantaneous plastic strain  $\kappa$ , the reloading curve is obtained by following external rule.

- When unloading is reversed to reloading with  $\kappa_{\max} \geq \kappa \geq \kappa_{\min}$  maintaining the previous  $\kappa_{\max}$  and  $\kappa_{\min}$ , the reloading curve is obtained by following the internal rule, and
- When the loading is continued while renewing the  $\kappa_{\max}$  value to instantaneous plastic strain  $\kappa$ , the loading curve  $\eta = f(\kappa)$  is followed.

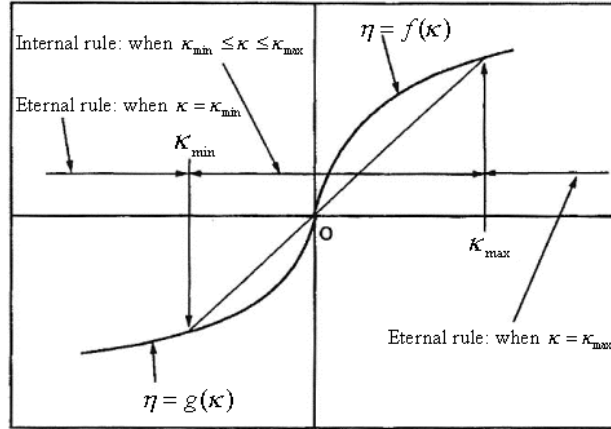


Fig. 4. Rule to choose either external or internal rule for given instantaneous plastic strain  $\kappa$

2. Stress-strain curves for unloading and so on are obtained as follows:
  - When loading is reversed to unloading while renewing the  $\kappa_{\max}$  value to the instantaneous plastic strain  $\kappa$ , the unloading curve is obtained by following external rule,
  - When loading is reversed to unloading with  $\kappa_{\max} \geq \kappa \geq \kappa_{\min}$  maintaining the previous  $\kappa_{\max}$  and  $\kappa_{\min}$ , the unloading curve is obtained by following the internal rule, and
  - When the unloading is continued while renewing the  $\kappa_{\min}$  value to instantaneous plastic strain  $\kappa$ , the unloading skeleton curve  $\eta = g(\kappa)$  is followed.

The rules are described below more specifically referring to Fig 3.

1. During the first primary loading from origin O ( $\kappa_0, \eta_0$ ), where  $\kappa_{\max} = \kappa_{\min} = 0$ , until point 'A', always  $\kappa_{\max} = \kappa$  and the stress-strain curve follows the loading skeleton curve  $\eta = f(\kappa)$ . At point 'A' ( $\kappa_A, \eta_A$ ), we have  $\kappa_{\max} = \kappa_A$  and  $\kappa_{\min} = \kappa_C$ .
2. When loading is reversed at point 'A', the unloading curve bound for point 'C' is obtained by following the external rule (with  $\kappa_{\max} = \kappa_A$ ) and using the known unloading skeleton curve  $\eta = g(\kappa)$  and the coordinate at point 'C' ( $\kappa_C, \eta_C$ ) as:

$$\frac{\eta - \eta_A}{n_1} = g\left(\frac{\kappa - \kappa_A}{n_1}\right) \quad (7.a)$$

$$n_1 = \frac{(-\eta_C) + \eta_A}{(-\eta_C)} = \frac{(-\kappa_C) + \kappa_A}{(-\kappa_C)} \quad (\geq 0) \quad (7.b)$$

3. When unloading continues passing point 'C', the stress-strain curve follows the unloading skeleton curve  $\eta = g(\kappa)$  with  $\kappa_{\max} = \text{instantaneous } \kappa$ .
4. Here, the target plastic strain  $\kappa_{\text{target}}$  is introduced, which is defined the value of  $\kappa$  at that point for which the stress-strain curve is bound after the loading direction is reversed. For unloading and reloading curves following the external rule,  $\kappa_{\text{target}}$  is equal to  $\kappa_{\min}$  and  $\kappa_{\max}$ , respectively. In Fig. 3  $\kappa_{\text{target}}$  for the unloading curve starting from point 'A' bound for point 'C' is  $\kappa_{\min} = \kappa_C$ .
5. In Fig. 3, when unloading is reversed to reloading at point 'B', where  $\kappa$  is between  $\kappa_{\min} = \kappa_C$  and  $\kappa_{\max} = \kappa_A$ , the reloading curve is obtained by following internal rule. The target point is assumed to be the same with the latest previous reversing point before point 'B' (i.e., point 'A'). Then, this reloading curve is obtained by scaling the loading skeleton curve as:

$$\frac{\eta - \eta_B}{n_2} = f\left(\frac{\kappa - \kappa_B}{n_2}\right) \quad (8.a)$$

$$n_2 = \frac{\eta_A - \eta_B}{\eta_d} = \frac{\kappa_A - \kappa_B}{\kappa_d} \quad (\geq 0) \quad (8.b)$$

where point 'd'  $(\kappa_d, \eta_d) =$  intersection of the straight line starting from the origin O while parallel to the straight line between points 'B' and 'A' with the loading skeleton curve  $\eta = f(\kappa)$ .

6. In Fig. 3 when the loading direction is reversed at point 'D', the re-unloading branch, which is bound for the latest previous point (i.e., point 'B'), is obtained by EQ. 7(a), but using another scaling factor  $n_3$  given below,

$$n_3 = \frac{(-\eta_C) + \eta_A}{(-\eta_C)} \frac{\eta_D - \eta_B}{\eta_A - \eta_B} = \frac{(-\kappa_C) + \kappa_A}{(-\kappa_C)} \frac{\kappa_D - \kappa_B}{\kappa_A - \kappa_B} \quad (\geq 0) \quad (9)$$

At point 'B', the re-unloading curve does not smoothly rejoin the previous unloading curve  $A \rightarrow B \rightarrow C$ . The unloading curve beyond point 'B' follows the curve  $A \rightarrow B \rightarrow C$ .

7. When following the internal rule, the  $\kappa_{\text{target}}$  value is always equal to the  $\kappa$  value at the latest previous reversing point (before the current revinging point). For example,  $\kappa_{\text{target}}$  is  $\kappa_A = \kappa_{\max}$  for the reloading branch  $B \rightarrow A$  and  $\kappa_B$  for the re-unloading branch  $D \rightarrow B$ .

8. Whenever the previous reversing point is passed, all the memory of previous cyclic loading history is erased. So, the reloading curve beyond Point B is bound for point 'A', not for point 'D'.

### 7. Stress-dilatancy relations (flow rule)

To convert the  $\eta \sim \kappa$  relation into a  $\sigma_v \sim \varepsilon_v$  relation, a flow rule, such as stress-dilatancy relation becomes necessary. The dilatancy behavior of sand has been studied by many researchers (Bolton, M. D., 1986, Tatsuoka, F., 1987). But for present study Rowe's stress-dilatancy relation is used. The Rowe's stress-dilatancy relation for plane strain condition is:

$$R = -KD \quad (10)$$

where,

$$R = \frac{\sigma_1}{\sigma_3} = \frac{1 + \sin \varphi_{mob}}{1 - \sin \varphi_{mob}}$$

$$K = \left( \frac{\sigma_1}{\sigma_3} \right)_{\varphi=\varphi_r} = \frac{1 + \sin \varphi_r}{1 - \sin \varphi_r}$$

$$D = -\frac{d\varepsilon_3^p}{d\varepsilon_1^p}$$

$\varphi_r$  = Residual angle of friction

Considering the plastic potential as Druker-Prager and a non-associated flow rule, it can be written,

$$\phi = \frac{1}{3}(\sigma_1 - \sigma_3) + \frac{1}{2}(\sigma_1 + \sigma_3)\sin \psi \quad (11)$$

From the definition of dilatancy angle the following relation can be obtained:

$$d\varepsilon_3^p = -\frac{1 + \sin \psi}{1 - \sin \psi} \quad (12)$$

Substituting eqn. 12,  $R$  and  $K$  into eqn. 10, the following equation can be obtained:

$$\frac{1 + \sin \psi}{1 - \sin \psi} = \frac{(1 + \sin \varphi_{mob})(1 + \sin \varphi_r)}{(1 - \sin \varphi_{mob})(1 - \sin \varphi_r)}$$

$$\text{Solving, } \sin \psi = \frac{\sin \varphi_{mob} - \sin \varphi_r}{1 - \sin \varphi_{mob} \sin \varphi_r} \quad (13)$$

Substituting eqn. 3 and eqn. 13 into eqn. 4, we get,

$$\xi = \frac{\sqrt{3}(\eta - \eta_r)}{\sqrt{3} + 3\eta_r - 6\sqrt{3}\eta\eta_r} \quad (14)$$

where,

$$\eta_r = \frac{2\sin \varphi_r}{\sqrt{3}(3 - \sin \varphi_r)}$$

This is the stress-dilatancy relation for loading and unloading skeleton curves. For loading and unloading curves, using eqn. 6, the stress-dilatancy relation becomes,

$$\xi = \frac{\sqrt{3}(\eta - n\eta_r)}{\sqrt{3} + 3n\eta_r - 6\sqrt{3}n\eta_r} \quad (15)$$

### 7.1 Material parameters

A hypothetical material is chosen to simulate the drained cyclic plane strain test results. In the following table the material parameters listed:

Table 1. Material parameters

Parameters	Symbol	Values
Elastic Shear modulus	$G_e$	7120 KPa
Elastic bulk modulus	$K_e$	25000 KPa
Peak Strength (Loading)	$\varphi_{pl}$	15°
Peak Strength (Unloading)	$\varphi_{pu}$	15°
Residual Strength (Loading)	$\varphi_{rl}$	12°
Residual Strength (Unloading)	$\varphi_{ru}$	12°
Cumulative Peak Plastic Strain (Loading)	$\kappa_{pl}$	0.1
Cumulative Peak Plastic Strain (Unloading)	$\kappa_{pu}$	0.1
Power of Hyperbolic Hardening Relation (Loading)	$m_l$	0.6
Power of Hyperbolic Hardening Relation (Unloading)	$m_u$	0.6

## 8. Results and discussions

To simulate the cyclic behavior of sand under plane strain condition, a hypothetical cyclic displacement is applied to a quadrilateral element. As a result, we found the stress-strain relationship of the sand undergoing cyclic loading. The results are plotted for various well-known relations. For each load step  $1e^{-5}$  mm/mm strain is applied in the  $\sigma_1$  direction and corresponding stress and strain matrix is found. From the total stress and strain matrix we found various required parameters. A set of results are simulated here. The graphs and their significances are stated below.

In Fig. 5 shear strain  $\gamma$  is plotted against the load steps. Thus we can visualize the cyclic behavior of strain applied.

In Fig. 6 the cumulative plastic strain ( $\kappa$ ) is plotted against the load step. Here we can see the accumulated plastic strain in loading direction is recovered in the reversed loading direction.

In Fig. 7 the  $\eta \sim \kappa$  relationship under cyclic loading is presented. Here, the  $\eta$  grows hyperbolically as plastic shear strain accumulates. It follows the Masing's rule and forms a closed loop.

In Fig. 8 the  $R \sim \kappa$  relationship under cyclic loading is illustrated. Here, the  $R = \sigma_1 / \sigma_3$  is the stress ratio. It is also a measure of the shear stress applied and have a value equal to

1 when  $\sigma_1 = \sigma_3$ . Its behavior also completely follows the Masing's rule and forms a closed loop.

In Fig. 9 the  $R \sim \gamma$  relationship under cyclic loading is plotted. It is similar to the  $R \sim \kappa$  relationship.

In Fig. 10 the  $\varepsilon_v \sim \gamma$  relationship under cyclic loading is demonstrated. The volumetric strain accumulation here follows the Rowe's stress-dilatancy relationship.

In Fig. 11 volumetric strain  $\varepsilon_v$  is plotted against the load steps. Thus we can visualize the cyclic behavior of the volumetric strain.

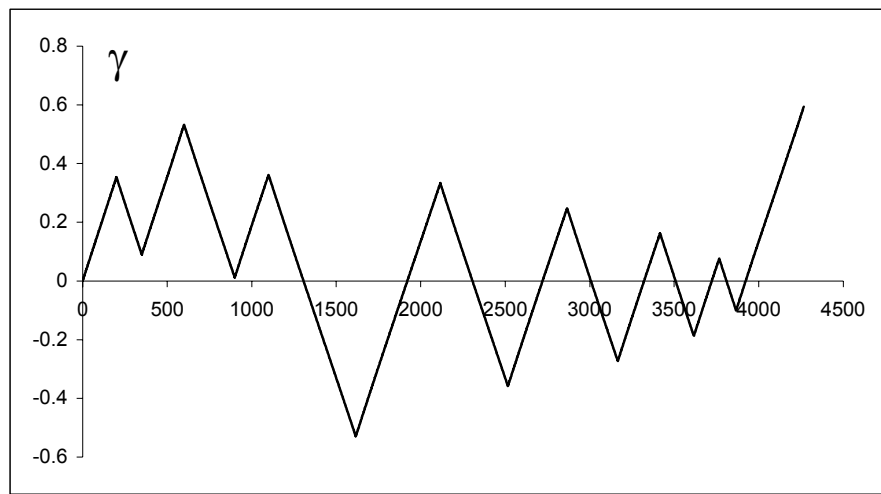


Fig. 5. Shear strain  $\gamma$  vs. load steps

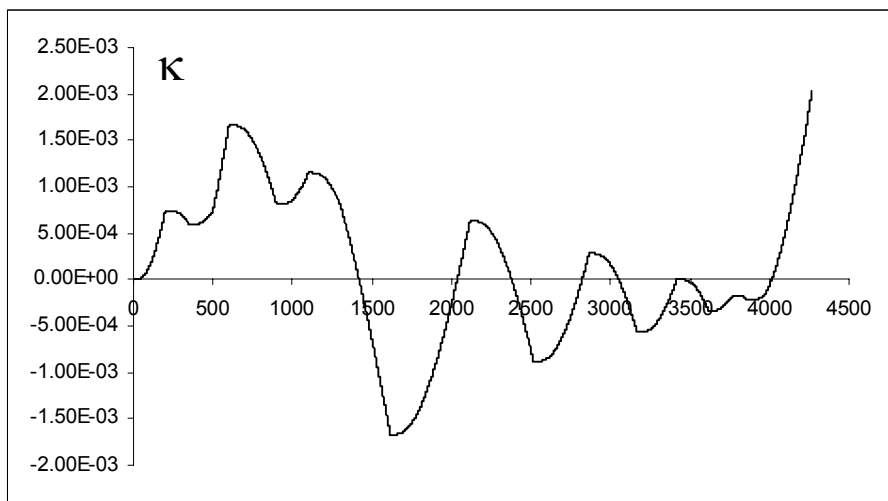


Fig. 6. Cumulative plastic strain  $\mathcal{K}$  vs. load steps

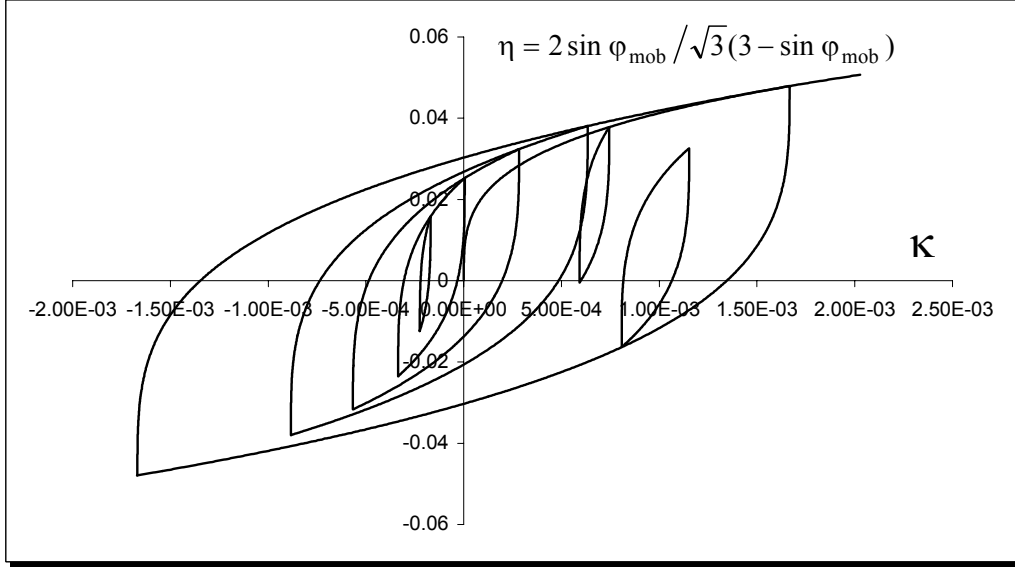


Fig. 7.  $\eta \sim \kappa$  curve

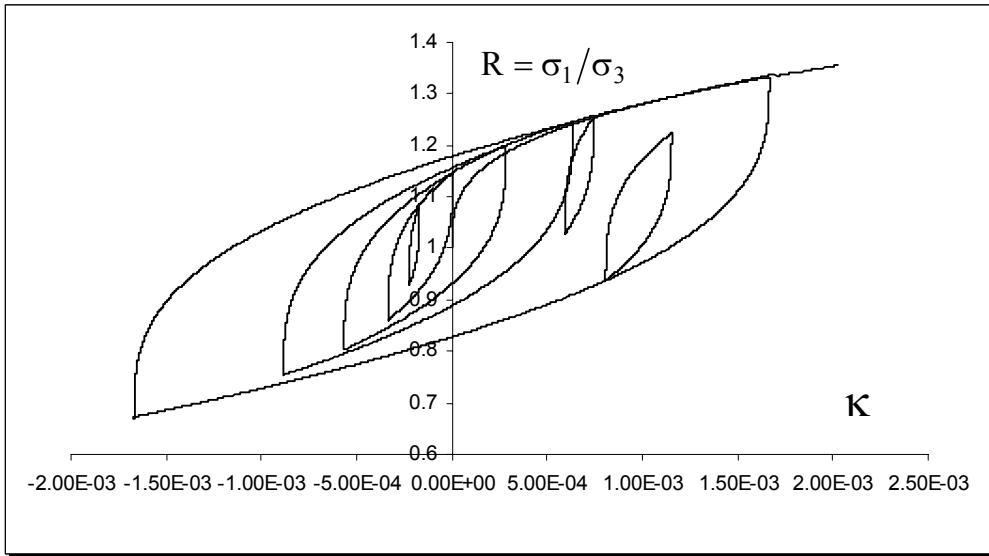


Fig. 8. Stress ratio  $R$  vs. cumulative plastic strain  $\kappa$

## 9. Conclusions

The following conclusion can be drawn from the results simulated by the model,

1. The relationship between stress ratio  $R = \sigma_1 / \sigma_3$  and shear strain  $\gamma = \varepsilon_1 - \varepsilon_3$  obtained from the drained cyclic plane strain test on a hypothetical pressure independent material performed at a constant  $\sigma_3$  is rather symmetric to the about the neutral axis of  $R = 0$ .

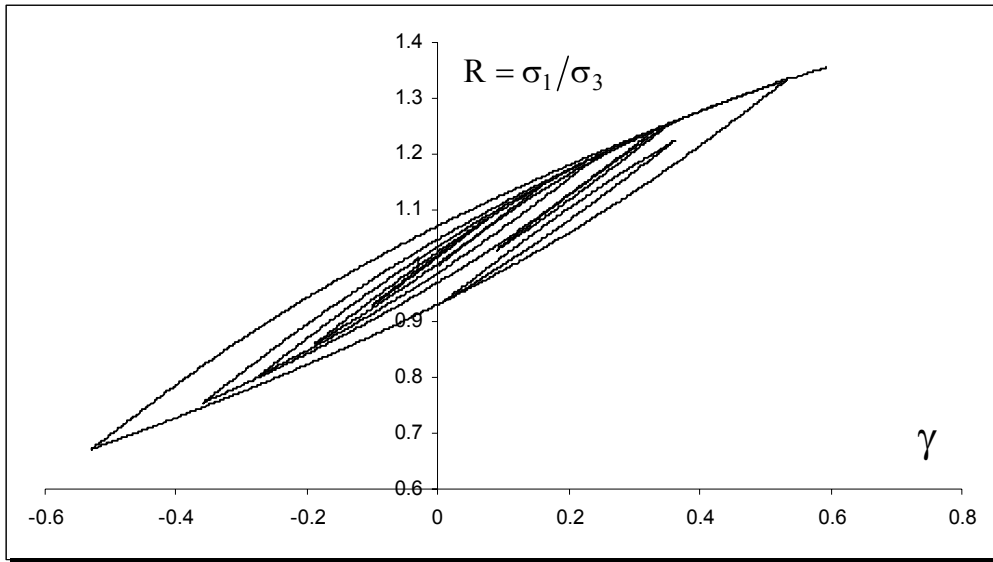


Fig. 9. Stress ratio  $R$  vs. shear strain  $\gamma$

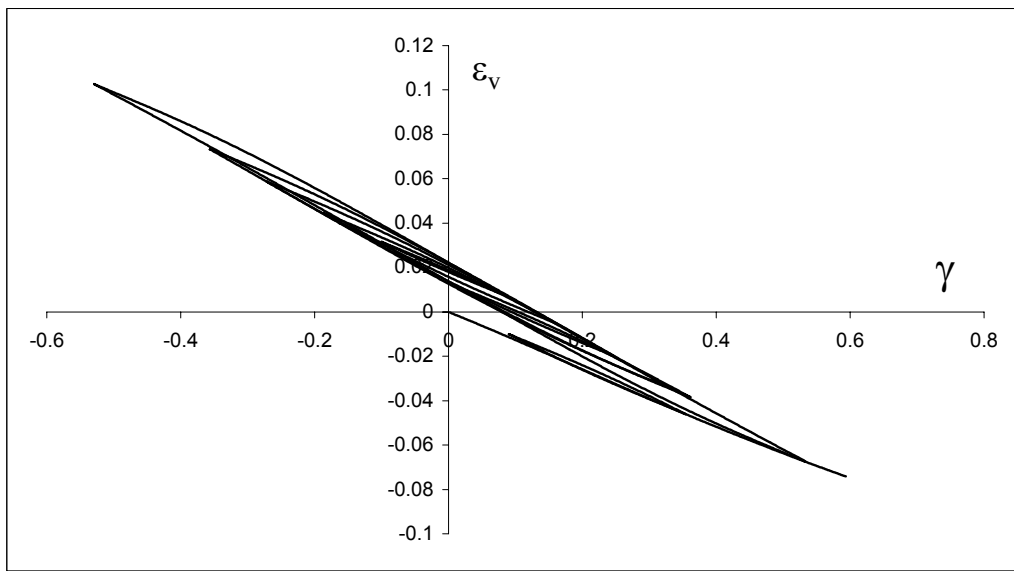


Fig. 10. Volumetric strain  $\varepsilon_v$  vs. shear strain  $\gamma$

2. The hyperbolic relationship (Tanaka) could simulate to a reasonable accuracy those  $\eta \sim \kappa$  relations. So, the simulated  $\eta \sim \kappa$  relations can be used as the skeleton curves in the simulation of the cyclic plane strain stress-strain behavior.
3. The proportional rule consisting of external and internal rule (Tatsuoka et al. 2003) formulated by modifying the original Masing's rule is used here. The proportional rule is more flexible and more general to simulate stress-strain relations of sand under various cyclic loading conditions, in particular when the

primary loading and unloading stress-strain relations are not symmetric about the neutral axis.

4. After necessary modification, the Rowe's stress-dilatancy relation could reasonably simulate the flow characteristics in cyclic plane strain loading.
5. Finally, the proposed framework can be well integrated with the finite element method (FEM) to solve the boundary value problems subjected to cyclic loadings.

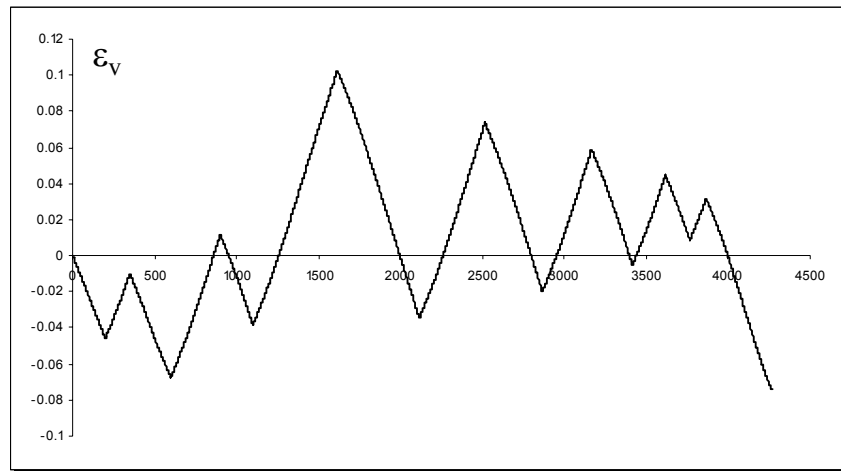


Fig. 11. Volumetric strain  $\epsilon_v$  vs. load steps

The model proposed here can well simulate the cyclic behavior of a hypothetical material, which is pressure independent. Thus, the model is a complete model for pressure independent material and with further modification it should be applied to pressure dependent materials. Also introducing the drag rule it will simulate the cyclic stress-strain behavior in which the stress amplitude increases at a decreasing rate during cyclic loading with constant strain amplitude.

### References

- Bolton, M.D. (1986). "The strength and dilatancy of sands", *Geotechnique*, 36, No. 1, 65-78.
- Hossain, M.R. (2005). "FE Modeling of the Stress-Strain Behavior of Sand in cyclic Plane Strain Loading", B. Sc. Engg. Thesis, Bangladesh University of Engineering and Technology.
- Montáns, F. J. (2000). "Bounding surface plasticity model with extended Masing's behavior", *Comput. Methods Appl. Mech. Engrg.*, 182, 135-162.
- Siddiquee, M.S.A. (1994). "FEM simulations of deformation and failure of stiff geomaterials based on element test results", D.Eng. dissertation, The University of Tokyo, Japan.
- Tanaka, T., "Elasto-plastic strain hardening-softening soil model with shear banding".
- Tatsuoka, F. (1987). "Discussion" on "The strength and dilatancy of sands", by Bolton, M.D., *Geotechnique*, 37, No. 2, 219-226.
- Tatsuoka, F., Jardine, R.J., Lo Presti, D.C.F., Di Benedetto, H., and Kodaka, T. (1999). "Characterizing the pre-failure deformation properties of geomaterials, Theme Lecture", *Proc. 14<sup>th</sup> ICSMFE*, Hamburg, 1997, 4, 2129-2164.
- Tatsuoka, F., Masuda, T., Siddiquee, M.S.A., and Koseki, J. (2003). "Modeling the stress-strain relation of sand in cyclic plane strain loading", *J. Geotech. Geoenv. Engrg., ASCE*, May, 450-467.